Influence of Porosity, Fiber Radius and Fiber Orientation on the Transport and Acoustic Properties of Random Fiber Structures

Hoang Tuan Luu, Camille Perrot, Raymond Panneton

Influence of Porosity, Fiber Radius and Fiber Orientation on the Transport and Acoustic Properties of Random Fiber Structures

Hoang Tuan Luu[1,2)], Camille Perrot[2)], Raymond Panneton[1)]

[1)] Groupe d'Acoustique de l'Université de Sherbrooke (GAUS), Department of Mechanical Engineering, Université de Sherbrooke, Québec J1K 2R1, Canada. raymond.panneton@usherbrooke.ca

[2)] Université Paris-Est, Laboratoire Modélisation et Simulation Multi Echelle, MSME UMR 8208 CNRS, 5 bd Descartes, 77454 Marne-la-Vallée, France. camille.perrot@u-pem.fr

Summary

The ability of air-saturated fibrous media to mitigate sound waves is controlled by their transport properties that are themselves controlled by the geometrical characteristics of their microstructure such as the open porosity, fiber radius, and fiber orientation. Here, micro-macro relationships are proposed to link these microstructural features to the macroscopic transport properties of random fiber structures. These transport properties are the tortuosity, the viscous and thermal static permeabilities, and the viscous and thermal characteristic lengths. First, representative elementary volumes (REVs) of random fiber structures are generated for different triplets of porosity, fiber radius and fiber orientation. The fibers are allowed to overlap and are motionless (rigid-frame assumption). The fiber orientation is derived from a second order orientation tensor. Second, the transport equations are numerically solved on the REVs which are seen as periodic unit cells. These solutions yield the transport properties governing the sound propagation and dissipation in the respective fibrous media. From these solutions, micro-macro relationships are derived to estimate the transport properties when the geometry of the fiber structure is known. Finally, these relationships are used to study the influence of the microstructural features on the acoustic properties of random fiber structures.

1. Introduction

The ability to tune the porosity, the fiber radius, and the fiber orientation of fiber structures make them attractive materials for sound absorption-based applications. These three geometrical characteristics affect the transport properties that govern the visco-inertial and thermal losses of sound waves in fiber structures. These transport properties are the tortuosity, the viscous and thermal static permeabilities, and the viscous and thermal characteristic lengths. Consequently, it is important to understand how the geometrical characteristics influence the anisotropic transport properties of random fiber structures.

In sound absorbing fibrous media, visco-thermal dissipation phenomena are mainly determined by permeability/resistivity of the porous sample, which gives rise to empirical models with versatile applications [1, 2]. As a general rule, the low frequency limit ($\omega \to 0$) of the dynamic viscous permeability $k(\omega)$ of the fibrous sample always

decreases with the increase of average angle θ between the fiber axis and the sound wave propagation direction [3, 4]. This microstructural effect results in a lower mean velocity $\langle \overrightarrow{v} \rangle$ in a viscous fluid flow solution of the Stokes equations,

$$\phi \left\langle \overrightarrow{v} \right\rangle = \frac{k(\omega)}{\eta} \overrightarrow{\nabla} p, \tag{1}$$

where ϕ is the open porosity, η is the dynamic viscosity of the saturating fluid and $\overrightarrow{\nabla} p$ is a macroscopic pressure gradient acting as a source term in the generalized Darcy law. The low frequency limit of the dynamic viscous permeability is called the static viscous permeability k_0. It is linked to the static airflow resistivity as $\sigma = \eta/k_0$, which is usually used in the acoustic literature [1]–[4].

At high frequencies ($\omega \to \infty$), the imaginary part of $k(\omega)$ dominates and the real distance traveled by the wave between two points is the rectilinear distance between them multiplied by $\sqrt{\alpha_\infty}$ because of the tortuosity α_∞ of the path [5]. The tortuosity is directly measurable from conductivity experiments or simulations [6]. This fact was

first pointed out by Rayleigh [7] and Brown [6]. The tortuosity also decreases with the average angle reduction ($\alpha_\infty \geq 1 \to 1$, when $\theta \to 0$) and with the porosity increase ($\alpha_\infty \geq 1 \to 1$, when $\phi \to 1$). The variation of Re[$k(\omega)$] arises from a combination of the inertial effect plus a dependence of the viscous boundary layer thickness $\delta_v = \sqrt{2\eta/\rho_0\omega}$, ρ_0 being the density of the fluid at rest. At high frequencies, the real part of $k(\omega)$ is given by

$$\lim_{\omega \to \infty} \mathrm{Re}\left[k(\omega)\right] = \frac{\phi}{2\Lambda\alpha_\infty}\delta_v^3, \qquad (2)$$

where Λ is the viscous characteristic length. The Λ parameter and its significance as a weighted measure of the pore volume-to-surface ratio was first emphasized by Johnson *et al.* [8, 9].

Diffusion controlled reactions can be simulated in microstructural models to provide estimates of the trapping constant Γ, or the so-called static thermal permeability $k_0' = 1/\Gamma$ ($k_0' \geqslant k_0$) [10], which represents the low frequency limit of the thermal response function,

$$\phi\langle\tau\rangle = \frac{k'(\omega)}{\kappa}\frac{\partial\langle p\rangle}{\partial t}, \qquad (3)$$

where $\langle\tau\rangle$ is the macroscopic excess temperature in fluid phase, $k'(\omega)$ is the dynamic thermal permeability, $\langle p\rangle$ is the macroscopic pressure and κ is the thermal conduction coefficient.

Johnson *et al.* [9] and Lafarge *et al.* [10] showed that $k(\omega)$ and $k'(\omega)$ can be adequately described by approximate but robust semi-phenomenological models based on more readily measurable physical properties (ϕ, α_∞, Λ, Λ', k_0, k_0'). Here, Λ' denotes the generalized hydraulic radius also known as the thermal characteristic length in the context of sound absorbing materials [11]. The results of Zhou and Sheng [5], on the universality properties of the dynamic permeability $k(\omega)$, suggest that the acoustic properties of fibrous media can be deduced from a limited amount of geometrical characteristics (fiber information orientation Ω_{zz}, fiber radius r_f, porosity ϕ, hydraulic radius Λ') and resulting transport information (static viscous permeability k_0, tortuosity α_∞, viscous characteristic length Λ, static thermal permeability k_0').

The use of even-order tensors was introduced by Advani and Tucker to describe the probability distribution function of fiber orientation in fiber materials [12]. The versatile modelling capability of tensors makes them appropriate to elucidate the effect of angular orientation on the sound propagation and dissipation mechanisms; this will be shown in this paper.

A thorough review of the literature was conducted by Tomadakis and Robertson [13] who compared many experimental and theoretical studies on the viscous permeability of various types of fiber structures. The data from these studies were presented in terms of dimensionless viscous permeability versus porosity to facilitate the comparison with theoretical predictions. They were categorized by the type of the fiber structure and flow configuration. The structures formed by cylindrical overlapping fibers

distributed randomly in 1, 2, or 3 directions were considered; the fibers being allowed to overlap freely in all the three cases. All one- and two-directional structures examined are statistically anisotropic, therefore the permeability was derived both parallel and perpendicular to their characteristic directions. It was found that the conjecture of Johnson *et al.* [8, 9] ($k_0 = \phi\Lambda^2/8\alpha_\infty$) provides very good permeability estimates in most cases, resulting in an overall ratio of the theoretical prediction to measurement close to 1.25 for the over 500 experimental points utilized. However, the predictions of all examined fiber structures and flow configurations also revealed a significant effect of fiber directionality on permeability (Figure 8 of [13]), an effect that can also be regarded as a specific mean to functionalize the fibrous material.

Starting from the comment that some non-woven fibrous materials yield a very low absorption contrast with X-rays, and therefore that usual computer tomography does not yield satisfying 3D images of the materials, Schladitz *et al.* [14] used 2D images of sections parallel and orthogonal to the flow direction obtained by classical light microscopy. The material was first infiltrated with a resin. Then, sections were cut, ground and polished. Repeated simulations of a stochastic model combined with image processing techniques gave evidence that the anisotropy parameter β of spatially stationary random system of lines (Poisson line process) can be successfully estimated from the number of fibers observed in sections parallel and orthogonal to the flow direction. This procedure corresponds to an experimental method available to estimate the orientation of fibers when 3D images are missing or failing to yield satisfying information. Additional mapping between the tensorial formalism and the Poisson line process leads to a common framework for the generation of disordered fiber structures, illustrating the crucial role of the parameter governing the orientation of fibers in transversely isotropic fibrous materials (Ω_{zz} as defined in Section II.B). The Poisson line process model was subsequently used by Jensen and Raspet [15] to investigate thermoacoustic properties of overlapping fibrous materials in order to test the prediction of analytical models [16, 17]. The parameters of the models (shape factors and relaxation times) are selected to best fit the numerical simulations that were made using a lattice Boltzmann approach.

In this paper, new numerical data are presented and used to systematically describe the anisotropic transport properties of sound absorbing fibrous media from geometrical information only. Rigid frame models will be examined with special attention to fiber orientation effect, and a large range of porosities will be studied. Section 2 presents the generation of Representative Elementary Volumes (REVs) of randomly overlapping fiber structures based on a parametrized fiber orientation. While Section 3 deals with the identification of the geometrical properties from the REVs, Section 4 deals with the identification of the transport properties. Finally, Section 5 summarizes the main micro-macro relationships developed in Sections 3

and 4, and these relations are applied to study the influence of the microstructural features on the acoustic properties of random fiber structures.

2. Random fiber structures

Like in previous studies [14, 15], a simple model for the fiber structure with the smallest possible number of parameters is considered. Following Schladitz *et al.* [14], the following assumptions were made. Compared to the sample size, the fibers are long and their curvature is negligible. There is no interaction between the fibers. Due to the production process, the fiber structure is macroscopically homogeneous and isotropic in the horizontal (xy-)plane. That is, the distribution properties of the random model are invariant by translations as well as rotations around the z-axis. Therefore, a detailed study of the effect of correlations between fibers is out of the scope of this work.

2.1. Orientation distribution function

For the purpose of the present research, the random fiber structures result from the successive generation of rigid uniform cylinders of the same diameter. The fibers are introduced at random locations with a uniform number of fibers per unit volume. A way to describe the orientation of a fiber is to associate a unit vector $\overrightarrow{p}$ to the fiber, as shown in Figure 1. A random fiber structure is therefore an arrangement of fibers for which the orientation distribution function is a defined function $\Psi(\varphi, \theta)$ of two variables describing the orientation of a single fiber. Examples are given in Figures 1 and 2. Note that in these figures, the x, y, z axes respectively correspond to unit vectors $\overrightarrow{e}_1$, $\overrightarrow{e}_2$, $\overrightarrow{e}_3$.

It is worth recalling that Tomadakis and Robertson [13] simulated one-, two-, and three- dimensional randomly overlapping fiber structures. However, these structures only corresponds to the three specific configurations of the fiber orientations shown in Figure 1b,c,d.

2.2. Orientation tensor

The use of tensors to describe fiber orientation of composite fibers was presented in a series of papers [18]–[21] and reviewed by Advani and Tucker [12]. The second-order orientation tensor is obtained by forming dyadic products of the vector $\overrightarrow{p}$ and then integrating the products with the distribution function over all possible directions,

$$\Omega_{ij} = \int p_i p_j \Psi(\overrightarrow{p}) \, \mathrm{d}\overrightarrow{p}, \tag{4}$$

where the set of all possible directions of $\overrightarrow{p}$ corresponds to the unit sphere, and the integral over the surface of the unit sphere is noted by

$$\int \mathrm{d}\overrightarrow{p} = \int_{\varphi=0}^{2\pi} \int_{\theta=0}^{\pi} \sin\theta \, \mathrm{d}\theta \, \mathrm{d}\varphi. \tag{5}$$

A fiber oriented at any angle (φ, θ) is undistinguishable from a fiber oriented at angle $(\varphi + \pi, \pi - \theta)$, so Ψ must satisfy

$$\Psi(\varphi, \theta) = \Psi(\varphi + \pi, \pi - \theta) \text{ or } \Psi(\overrightarrow{p}) = \Psi(-\overrightarrow{p}). \tag{6}$$

Ψ must be normalized, since every fiber has some orientation,

$$\int_{\varphi=0}^{2\pi} \int_{\theta=0}^{\pi} \Psi(\varphi, \theta) \sin(\theta) \, \mathrm{d}\theta \, \mathrm{d}\varphi = \int \Psi(\overrightarrow{p}) \, \mathrm{d}\overrightarrow{p} = 1. \tag{7}$$

Because the distribution function is even [Equation (6)], only the even-order tensors are of interest (the odd-order integrals are zero). Using Equation (7), the integral over all $\overrightarrow{p}$ weighted by $\Psi(\overrightarrow{p})$, which appears in Equation (4) becomes, for a discrete set of fibers,

$$[\Omega] = \frac{1}{N_f} \sum_{i=1}^{N_f} \left[\begin{array}{c} \sin^2\theta^{(i)}\cos^2\varphi^{(i)} \\ \sin^2\theta^{(i)}\cos\varphi^{(i)}\sin\varphi^{(i)} \quad \cdots \\ \sin\theta^{(i)}\cos\theta^{(i)}\cos\varphi^{(i)} \end{array} \right. \tag{8}$$

$$\left. \begin{array}{cc} \sin^2\theta^{(i)}\cos\varphi^{(i)}\sin\varphi^{(i)} & \sin\theta^{(i)}\cos\theta^{(i)}\cos\varphi^{(i)} \\ \cdots \quad \sin^2\theta^{(i)}\sin^2\varphi^{(i)} & \sin\theta^{(i)}\cos\theta^{(i)}\sin\varphi^{(i)} \\ \sin\theta^{(i)}\cos\theta^{(i)}\sin\varphi^{(i)} & \cos^2\theta^{(i)} \end{array} \right],$$

where N_f is the total number of fibers, $\theta^{(i)}$ is the vertical orientation angle, and $\varphi^{(i)}$ is horizontal orientation angle. Here, $[\Omega]$ is completely symmetric, and from the normalization condition (7) it can be shown that $Trace[\Omega] = 1$. $[\Omega]$ constitutes the most concise nontrivial description of the orientation. Assuming a transversely isotropic material, $[\Omega]$ is completely determined by Ω_{zz}. Varying the value of Ω_{zz} from planar ($\Omega_{zz} = 0$) to aligned ($\Omega_{zz} = 1$) random fibers, one can study the influence of fiber orientation on the transport properties of fibrous media. This was simply done by adjusting the mean μ_θ and standard deviation σ_θ of a normal distribution of angle θ with a uniform random orientation of angle φ. All the corresponding coefficients are reported in Table I.

The choice of the distributions on θ and φ is based on the experimental knowledge acquired by the authors on several random fibrous materials using SEM images. From the authors' knowledge, the following modelling assumptions can be formulated: (i) the horizontal angle follows a uniform distribution between 0 and 180 °; (ii) as the number of analysed fibers increases, the probability density function of the vertical angle is approximately normal (with a mean value generally centered at 90° in most cases). An example of such a distribution obtained by SEM image analysis is given elsewhere [22].

2.3. Generation of random fiber structures

Here is a short description of the algorithm which is fully detailed elsewhere [22], and displayed in Figure 3. The algorithm is used to generate a representative elementary volume (REV) for a given fiber orientation coefficient Ω_{zz}. The algorithm allows fibers to overlap as in [13], [14] and [15]. This can be questionable since in reality the fibers
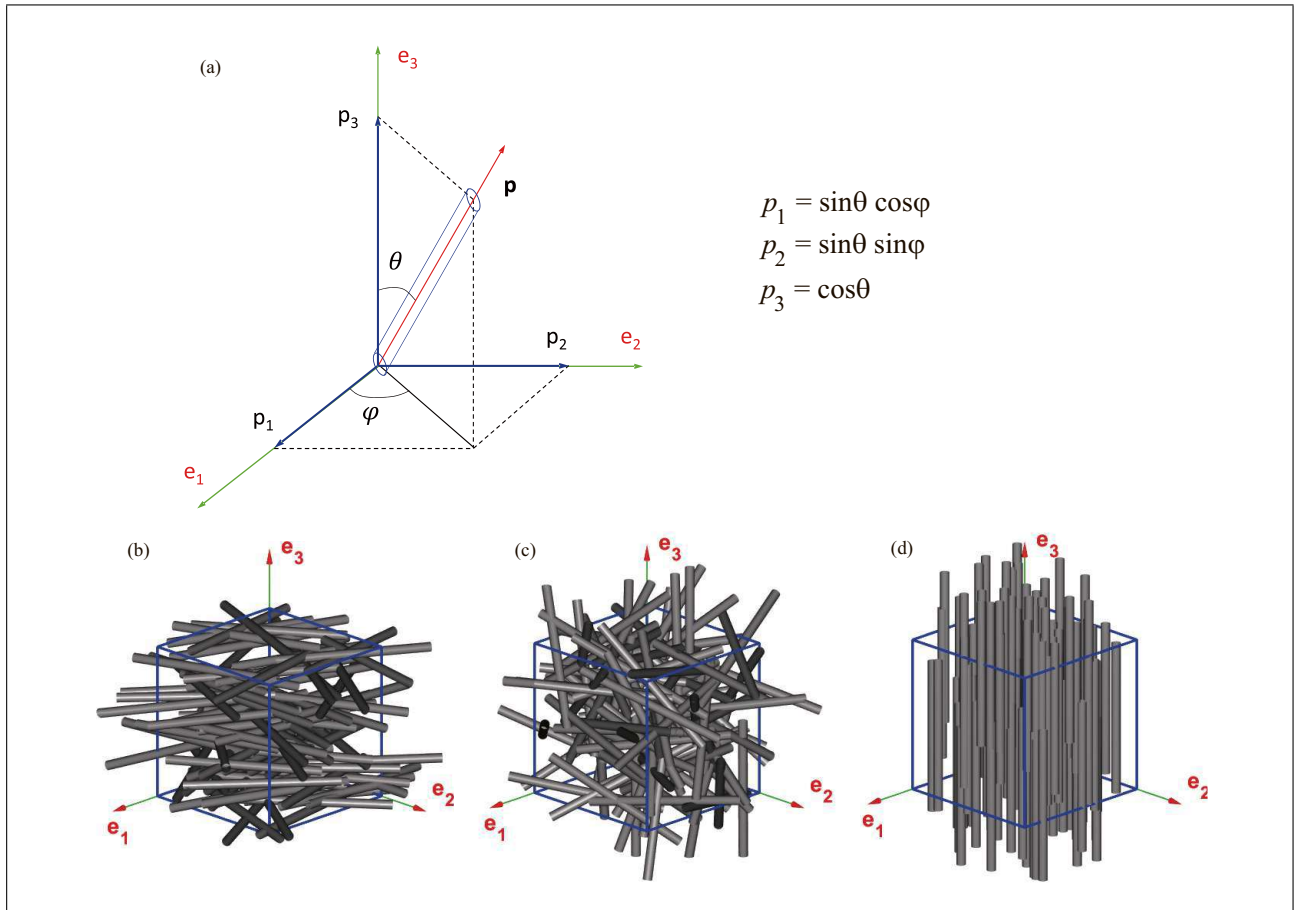
Figure 1. (Colour online) (a) The fiber definition in the polar coordinates (φ, θ). Examples of typical randomly overlapping fiber structures. (b) Two-directional (2-d) random fiber structures where fibers are in parallel planes (transversely isotropic); this configuration corresponds to $\Omega_{zz} = 0$ (layered fibrous media). (c) Three-directional (3-d) random fiber structures where fibers are randomly positioned and oriented in the three-dimensional space; this configuration corresponds to $\Omega_{zz} = 1/3$ (isotropic fibrous media). (d) One-directional (1-d) random fiber structures where fibers are parallel to each other, with their traces randomly positioned in the plane Oxy; this configuration corresponds to $\Omega_{zz} = 1$ (aligned fibrous media).

Table I. Coefficient Ω_{zz} of the second-order transversely isotropic fiber orientation tensor and the corresponding mean μ_θ and standard deviation σ_θ adjusted assuming that θ is described by a normal distribution function and φ by a uniform distribution function.

Ω_{zz}	0	0.1	0.2	0.3	0.4	0.5	0.6	0.7	0.8	0.91	1
$\mu_\theta(^o)$	90	90	90	90	90	45.18	33.48	14.22	0	0	0
$\sigma_\theta(^o)$	0	19.17	29.98	38.88	51.50	171.18	29.98	36.18	28.80	19.08	0

can not physically interpenetrate. However, since they can deform, two fibers can be crushed one on the other.

As a general rule, a characteristic fiber radius r_f and a target open porosity ϕ are imposed. The position of a fiber is represented by the location $\overrightarrow{r}(x, y, z)$ of its center and by a set (φ, θ) of two angles that give the orientation of its axis with respect to the coordinate system. The fibers are generated in a square vertical box, as shown in Figures 1 and 2. The numerical calculations of the properties of the fiber structure are conducted in an elementary volume box of size $L^{(i)}$, where i represents the ith iteration on the box size. At the initial iteration, the box size is set to 100 μm, and will be iteratively increased by a value $\Delta L = 10$ μm.

This domain typically contains a solid volume of fibers equal to

$$V_f^{(i)} = (1 - \phi) L^{(i)3}. \qquad (9)$$

To identify the number of fibers of radius r_f that are required to meet this volume $V_f^{(i)}$, the number of fibers randomly generated in the box, following the predetermined Ω_{zz} coefficient, is iteratively increased. The iteration is stopped when for j fibers the solid volume of fibers $V_f^{(j)}$ is greater or equal to $V_f^{(i)}$. Here, $V_f^{(j)} = \pi r_f^2 \Sigma_1^j(l_f^{(k)})$, where $l_f^{(k)}$ is the length of the kth fiber generated during the process at iteration j. From the found volume $V_f^{(j)}$, the actual porosity $\phi^{(i)}$ of the elementary volume box i filled with
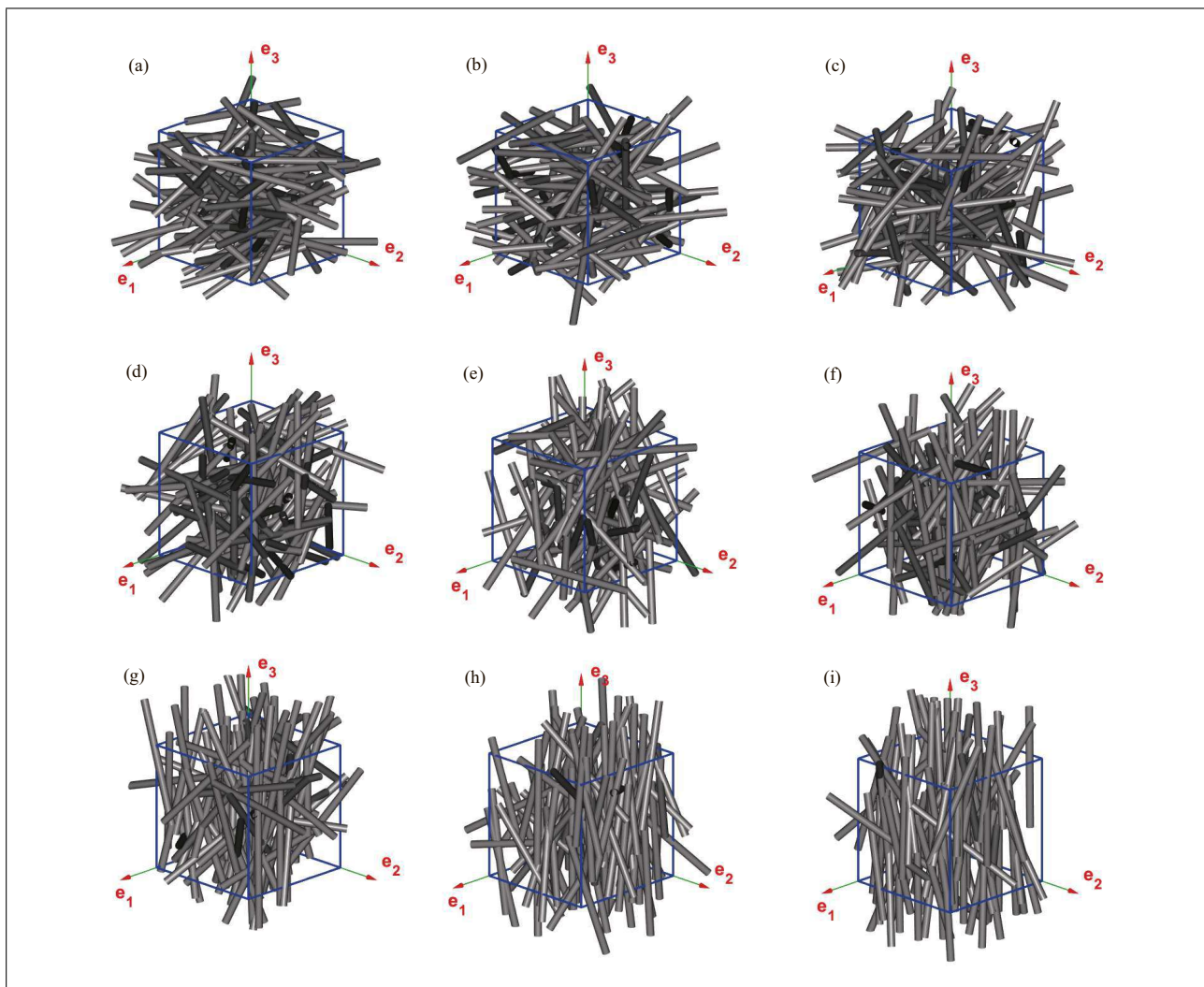
Figure 2. (Colour online) Various configurations corresponding to the variation of fiber orientation states with Ω_{zz} ranging from 0.1 to 0.9, respectively.

j fibers is compared to the expected value ϕ. If the relative error of the actual porosity is smaller than tolerance ε, then the convergence criterion on iteration *i* is finally met, and the current elementary volume box of size $L^{(i)}$ is the REV - its actual porosity is ϕ_{REV} and it contains *j* fibers. From this REV, numerical calculations are performed to retrieve the geometrical and transport properties. In practice, since there are variations between randomly generated fibrous networks for the same number of fibers and Ω_{zz} coefficient, the actual porosity that is used in the convergence criterion is an averaged value over 1000 realizations of the conditional loop over *j* - see counted loop over *m* in Figure 3. As a general trend, the size of the representative elementary volume L_{REV} is linearly decreasing with increasing porosity (at a given ε), and the smaller is ε the higher is L_{REV}. For the range of studied porosities, with $0.75 \leq \phi \leq 0.99$, the value $L_{REV} \leq 500\,\mu$m is large enough to ensure that $\varepsilon = 0.003$.

Note that the results presented in this study were conducted on a REV with $L_{REV} = 500\,\mu$m, a number of fibers $N_f = 68$ and a fiber radius varying between 4.3 μm and 19.23 μm to cover the porosity range $0.75 \leq \phi \leq 0.99$ (within $\varepsilon = 0.003$). For instance, at $\phi = 0.9$, $r_f = 11.1$ μm and $L_{REV} \approx 45r_f$. In practice, a numerical approach was used to determine the final volume and wet surface area of the resulting fiber webs, because there generally exists some overlaps between fibers.

3. Identification of the geometrical properties

The simplest geometrical properties of a random fiber structure are the characteristic fiber radius r_f, open porosity ϕ, and thermal characteristic length Λ'. Since r_f and ϕ are two input parameters of the REV generation (see Section 2.3), they are either imposed or obtained by measurements. They are imposed when one wants to study their effects on the acoustic properties, and they are measured when one wants to predict the acoustic or transport properties of an existing material. In the latter case, the characteristic fiber radius can be obtained from image analysis or the manufacturing process, and the open porosity
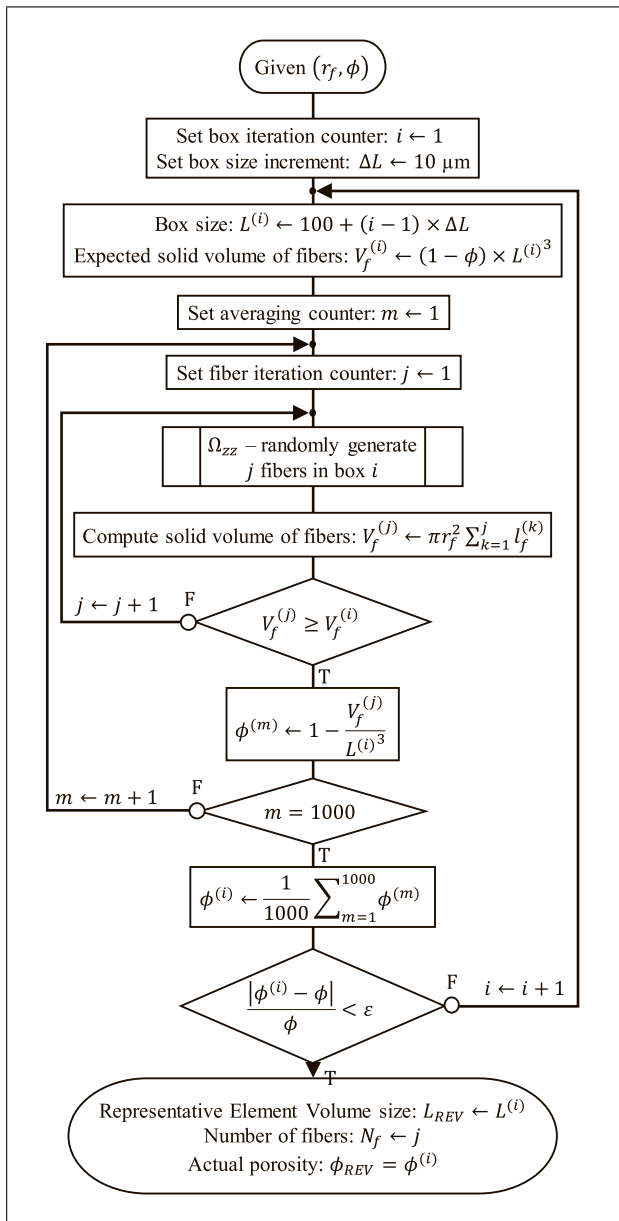
Figure 3. Algorithm for the determination of REV.

measured from existing methods [24]–[26]. Additionally, it is worth mentionning that for polydisperse and bidisperse fiber structures, it was shown that the weighted fiber radius can be used as the characteristic fiber radius [27].

The only geometrical property that remains to be identified is Λ'. This property is defined as twice the ratio between the fluid phase volume V_p and the wet solid surface area of the fibers S_w,

$$\Lambda' = \frac{2V_p}{S_w}.$$ (10)

In this study, each constructed REV is discretized by volume finite elements. Consequently, V_p and S_w are directly computed on each discretized REV, and Λ' deduced from the previous equation. The numerically computed ratios between the thermal characteristic length and the characteristic fiber radius Λ'/r_f are plotted in Figure 4 as a func-
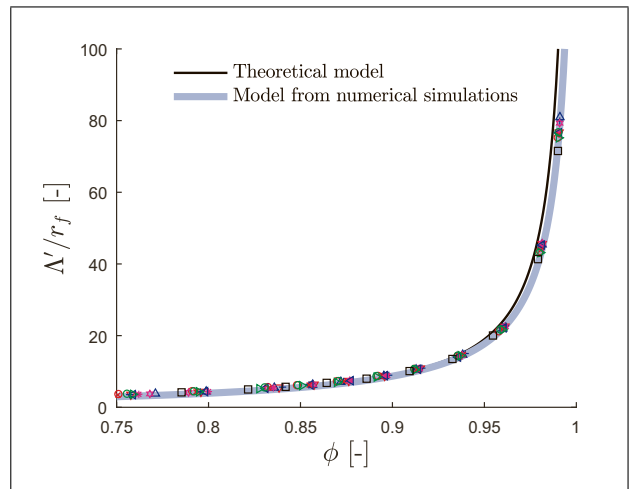

Figure 4. (Colour online) Normalized thermal characteristic length Λ'/r_f as a function of the open porosity ϕ. The symbols indicate the statistically averaged orientation of fibers as determined by the value of Ω_{zz}: $\Omega_{zz} = 0$ (∘), $\Omega_{zz} = 0.1$ (▽), $\Omega_{zz} = 0.2$ (△), $\Omega_{zz} = 0.3$ (+), $\Omega_{zz} = 0.4$ (#), $\Omega_{zz} = 0.5$ (∗), $\Omega_{zz} = 0.6$ (◂), $\Omega_{zz} = 0.7$ (×) $\Omega_{zz} = 0.8$ (∘), $\Omega_{zz} = 0.9$ (▸), $\Omega_{zz} = 1$ (□). The continuous curve corresponds to the theoretical model, Equation (11). The thick curve corresponds to the corrected model for overlapping fibers, Equation (12).

tion of the porosity for the various fiber orientations. As expected, all of the generated fiber structures follow the same behavior, with a nonlinear increase of Λ'/r_f as the fibrous media become more porous. Λ'/r_f is roughly independent on the angular orientation Ω_{zz}. Assuming that the fibers do not overlap, one can derive from Equation (10), a theoretical expression for this normalized length in function of the open porosity. It is given by

$$\frac{\Lambda'}{r_f} = \frac{\phi}{1-\phi}.$$ (11)

If the fibers are allowed to overlap, one can show from Equation (10) that an additional term would appear in the denominator of Equation (11). This term would depend on the r_f/L ratio, the number of intersections, and their corresponding shape (ex.: shape formed by intersection of two oblique fibers). The latter properties are difficult to evaluate on the studied REVs; however, the influence of the intersections can be taken into account by a correction term c in the denominator of Equation (11). Consequently, a better model to fit the numerical data obtained for our randomly overlapping fiber structures is given by

$$\frac{\Lambda'}{r_f} = \frac{\phi}{1-\phi+c}.$$ (12)

This expression is plotted on Figure 4. One can note that Equation (12) fits with the numerically calculated normalized characteristic thermal lengths, in which the value of c represents the fiber intersection intensity. By using a simple fit from the simulation results, we obtain $c = 0.0036$.

Thus, it can be concluded that a good approximation of Λ' can be deduced from r_f and ϕ by Equation (12) when

the characteristic fiber radius and porosity are imposed, or known from measurements.

4. Identification of the transport properties

In this section, the macroscopic effective coefficients for the basic transport processes by conduction, convection and diffusion- controlled reactions in random networks of fibers are studied. The governing equations and their solution methods are briefly recalled in this section. They are detailed in an earlier paper [22]. In all cases, the macroscopic coefficients are deduced by integrating the local fields, obtained by solving the transport equations at the pore scale. Since the webs are macroscopically homogeneous, they are considered as infinite periodic media, made of identical unit cells. The unit cells are the REVs generated as described in section II. Periodicity conditions along the x, y, and z axes were applied when computing the transport properties.

4.1. Tortuosity and viscous characteristic length

4.1.1. Theoretical framework

Electric conduction is governed by the following set of equations,

$$\vec{E} = -\vec{\nabla}\pi + \vec{e}, \qquad \vec{\nabla}\cdot\vec{E} = 0, \qquad (13)$$

where $\vec{E}$ and π are respectively the local values of the electric field and microscopic potential in the fluid, and $\vec{e}$ is a specific macroscopic electric field. $\vec{E}$ satisfies the no-flux boundary condition at the wall $\partial\Omega$ when the solid phase is assumed to be insulating,

$$\vec{E}\cdot\vec{n} = 0, \qquad (14)$$

where $\vec{n}$ is the unit normal vector to $\partial\Omega$. π is assumed to be spatially periodic with a period Ω in the three directions of space.

The quantities $\vec{E}$ and $\vec{e}$ are related by the symmetric positive definite tortuosity tensor $\alpha_{\infty ij}$,

$$e_i = \alpha_{\infty ij}\left\langle E_j \right\rangle, \qquad (15)$$

which depends only upon the geometry of the medium. Typically, for an isotropic random medium, $\alpha_{\infty ij}$ is a spherical tensor equal to $\alpha_\infty I$. For transversely isotropic fiber webs, the x and y directions play equivalent roles, but a different behavior along the z axis is expected. In the following, $\alpha_{\infty xy}$ denotes the average of the tortuosities along the x and y axes, which were found equal within the statistical fluctuations, and $\alpha_{\infty z}$ denotes the tortuosity in the vertical direction. The mean value over the three axes is denoted $\overline{\alpha}_\infty$.

The viscous characteristic length Λ, introduced by Johnson *et al.* [8] and applicable to any kind of porous media, is defined as

$$\Lambda = 2\frac{\int_\Omega \|\vec{E}\|^2\,\mathrm{d}V}{\int_{\partial\Omega} \|\vec{E}\|^2\,\mathrm{d}S}. \qquad (16)$$

Table II. Coefficients of polynomial $P(\Omega_{zz})$ used to correlate the tortuosity tensor $\alpha_{\infty ij}$ and viscous characteristic length tensor Λ_{ij} to the porosity ϕ and fiber orientation Ω_{zz}. Polynomial is of the form $A\Omega_{zz}^2 + B\Omega_{zz} + C$.

	A	B	C
$\alpha_{\infty xy}, \Lambda_{xy}$	0.2631	0.2895	0.5957
$\alpha_{\infty z}, \Lambda_z$	-0.0596	-0.9994	1.0590
$\overline{\alpha}_\infty$	-	-	0.7659

It is an effective pore-volume-to-surface ratio wherein each volume or area element is weighted according to the local value of the electric field $\vec{E}$, which would exist in the absence of a surface mechanism. Λ is a characteristic parameter of the geometry of the porous medium. This length can be derived from the numerical solution of the Laplace's equation in the pore space and used for the analysis of transport properties. The value of Λ obtained when setting $\vec{e}$ along the x and y directions is denoted by Λ_{xy}, while Λ_z corresponds to the z direction.

4.1.2. Numerical results and discussions

The calculations of the tortuosity tensor $\alpha_{\infty ij}$ were performed for the fiber structures described above. The purpose is to obtain a description for all types of random fibrous media using their single-geometry characteristics such as the porosity ϕ and the fiber orientation Ω_{zz} assuming transverse isotropy.

A study of the possible anisotropy of the results is first conducted. Figure 5 shows that, while the averaged tortuosity $\overline{\alpha}_\infty$ is fewly sensitive to Ω_{zz}, the transverse tortuosity $\alpha_{\infty xy}$ and longitudinal tortuosity $\alpha_{\infty z}$ are very sensitive to Ω_{zz}. As a general trend, it can be noted that fibers that are orthogonal to the direction of wave propagation yield higher tortuosity values than fibers that are parallel to the direction of wave propagation.

One popular empirical model for the determination of the tortuosity of porous media is the Archie's law given by $\alpha_\infty = (1/\phi)^\gamma$, where γ is a constant which depends on the microstructure of the porous medium. In our randomly overlapping fiber structures of transverse isotropy, the microstructure depends on the direction of the flow (along z or xy) and the fiber orientation coefficient Ω_{zz}. To extend Archie's law to our numerical results, the following expression is proposed:

$$\alpha_\infty = \left(\frac{1}{\phi}\right)^{P(\Omega_{zz})} \quad \text{(valid for } 0.75 \leqslant \phi \leqslant 1\text{)}, \qquad (17)$$

where $P(\Omega_{zz})$ is a polynomial of the second order whose coefficients are obtained by a nonlinear curve-fitting on our numerical results in a least-square sense. For $\alpha_{\infty xy}$ and $\alpha_{\infty z}$, the polynomial coefficients are given in Table II. Except for strongly aligned fiber networks with $\Omega_{zz} = 0.9$ and $\Omega_{zz} = 1$, the effect of fiber orientation is barely visible on $\overline{\alpha}_\infty$ as shown in Figure 5c. Consequently, a constant value $P(\Omega_{zz}) = 0.7659$ can be used in Equation (17) for
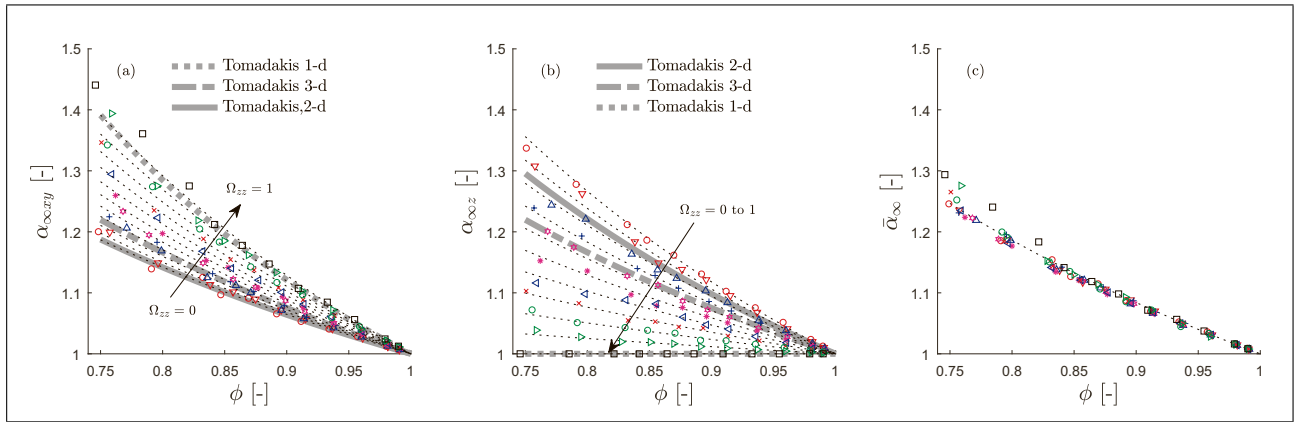
Figure 5. (Colour online) The tortuosities (a) $\alpha_{\infty xy}$, (b) $\alpha_{\infty z}$, and (c) $\overline{\alpha}_{\infty}$ as a function of porosity ϕ. Same convention of colors and symbols as in Figure 4. The symbols refer to numerically computed values. Dotted lines are estimates obtained by the micro-macro relationship, Equation (17). Thick gray lines refer to Tomadakis and Robertson's model (Equation(11) and Table 1 of [13]).

$\overline{\alpha}_{\infty}$. This value is also obtained by the same curve-fitting on all the numerical data.

Tortuosity estimates obtained with Equation (17) are plotted in Figure 5 (dotted lines). These estimates are also compared with results obtained by Tomadakis and Robertson [13]. Based on random-walk simulations on three specific types of randomly overlapping fiber structures (1-d, 2-d and 3-d), they derived a curve-fit relationship based on a generalization of the Archie's law. These fiber structures are similar to our configurations with $\Omega_{zz} = 1$, $\Omega_{zz} = 0$, and $\Omega_{zz} = 1/3$, respectively. As shown in Figure 5, good correlations are obtained for these three specific cases. The worst comparison is for $\alpha_{\infty z}$ with $\Omega_{zz} = 0$ (2-d, red circles). In this case, the Tomadakis and Robertson's model predicts tortuosity values smaller than our results. The comparison of the results of this work to the data of the literature reveals that the random-walk simulation results provide accurate predictions of the tortuosity of random fibrous structures in most cases - except for the flow perpendicular to two-directional randomly overlapping fiber structures - with the deviation increasing at low porosities (Figure 5b with $\Omega_{zz} = 0$, red circles). The latter corresponds to the situation where the cross-sectional area of the pore space varies relatively fast as one moves away from the throat. This indicates that the diffusional estimates of the tortuosity might not be accurate enough if the throat region differs significantly from the straight-tube-like model

As in the case of the tortuosity α_{∞}, the purpose of the next analysis is to obtain a description for the viscous characteristic length Λ for all random fibrous media as a function of the microstructural features. The numerical calculations were performed on the same REVs that were used for the tortuosity tensor analysis. The numerically computed thermal characteristic length Λ' normalized by the values of Λ_z and Λ_{xy} are shown in Figure 6 as a function of the porosity ϕ. One can note that the upper ($\Lambda'/\Lambda \approx 2$) and lower ($\Lambda'/\Lambda = 1$) bounds found here are consistent with those published in [11] (Equation 49) for fibers perpendicular and parallel to the plane wave propagation direction ($\overrightarrow{e}_3$).

Along direction $\overrightarrow{e}_3$, one can observe that there is no dependence of Λ'/Λ_z with ϕ. This is almost the case along the transverse direction for Λ'/Λ_{xy}; however, as the angular orientation increases, the ratio tends to increase with decreasing porosity. Indeed, Λ is an effective pore size of dynamically connected pore regions that contribute the most to fluid transport (an effective surface-to-pore volume wherein each area or volume element is weighted according to the local value of $\overrightarrow{E}$, Equations 13 and 14). This weighting eliminates contributions from the isolated regions of the pore space that do not contribute to transport. This effect is strong when the fibers are perpendicular to flow direction, and increases as the porosity of the fibrous material decreases.

For a certain types of porous media, Johnson *et al.* [8] have shown that the viscous characteristic length can be expressed by

$$\Lambda'/\Lambda_z = -\frac{\log(F)}{\log(\phi)}, \tag{18}$$

where $F = \alpha_{\infty}/\phi$ is the formation factor. Substituting the expression of the formation factor in Equation(18), together with relationship of Equation(17), the previous equation readily gives the following micro-macro relationship:

$$\Lambda'/\Lambda = 1 + P(\Omega_{zz}) \quad \text{(valid for } 0.75 \leqslant \phi \leqslant 1\text{)}. \tag{19}$$

Here $P(\Omega_{zz})$ is the same polynomial as in Equation (17) with coefficients defined in Table II for Λ_z and Λ_{xy}.

Estimates of Λ'/Λ_z and Λ'/Λ_{xy} obtained with Equation (19), and the respective coefficients of Table II, are plotted in Figure 6 (dotted lines). These estimates are also compared with results obtained by Tomadakis and Robertson [13] for the three specific randomly overlapping 1-d, 2-d and 3-d fiber structures. Again, good correlations are obtained, except for Λ'/Λ_z for the 2-d structure (red circles in Figure 6a). In this case, the ratio is lower than the expected ratio of 2. The reasons previously given for the tortuosity still apply here to explain this discrepancy.
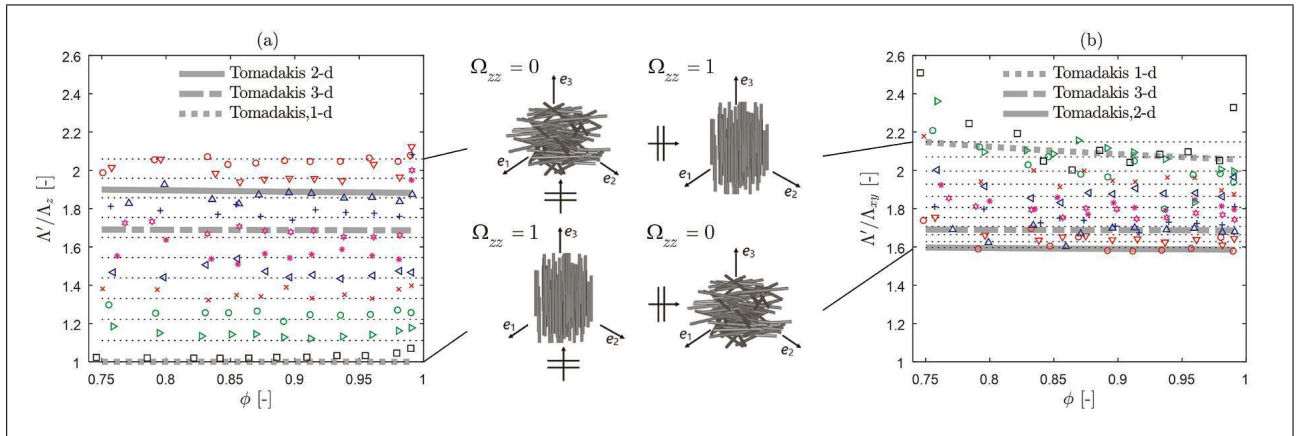
Figure 6. (Colour online) Characteristic length ratio (a) Λ'/Λ_z and (b) Λ'/Λ_{xy} as a function of porosity ϕ. Same convention of colors and symbols as in Figure 4. The symbols refer to numerically computed values. Dotted lines are estimates obtained by the micro-macro relationship, Equation (19). Thick gray lines refer to Tomadakis and Robertson's model (Equation(10), Equation(11) and Table 1 of [13]).

It is worth mentioning that the results by Tomadakis and Robertson also show that the Λ'/Λ_{xy} ratio is no more constant as the fiber orientation coefficient approaches 1. For higher orientation coefficients, it tends to increase as porosity decreases.

The results above confirm the accuracy of the numerical model and indicate that it captures the essential physics of the fluid-structure interaction as frequency tends to infinite. We therefore conclude that the proposed micro-macro relationships may be regarded as generally valid.

4.2. Static viscous permeability

4.2.1. Theoretical framework

Permeability can be derived from the solution of Stokes equations,

$$\eta\nabla^2\overrightarrow{v} - \overrightarrow{\nabla}p = -\overrightarrow{G}, \qquad \overrightarrow{\nabla}\cdot\overrightarrow{v} = 0, \qquad (20)$$

where $\overrightarrow{v}$, p and η are the velocity, pressure, dynamic viscosity of the fluid, respectively, and $\overrightarrow{G} = \overrightarrow{\nabla}p^m$ is a macroscopic pressure gradient acting as a source term. The velocity $\overrightarrow{v}$ verifies the non-slip boundary condition on the wet surface of the fibers

$$\overrightarrow{v} = 0 \quad \text{on} \quad \partial\Omega. \qquad (21)$$

Because of the spatially periodic character on the large scale of the porous media, $\overrightarrow{v}$ and p are assumed to be spatially periodic functions with a period equal to the cell size Ω.

The system of Equations (20) - (21) with the periodic boundary condition is numerically solved for a specified macroscopic pressure gradient $\overrightarrow{G}$ on the REVs, which is set to be equal to a prescribed constant vector. Since Equations (20) and (21) form a linear system of equations, it can be demonstrated that $\langle\overrightarrow{v}\rangle$ is a linear function of $\overrightarrow{G}$. These quantities are related by the permeability tensor k_{0ij},

$$k_{0ij} = \phi\left\langle k^*_{0ij}\right\rangle, \qquad (22)$$

where k_{0ij} is a symmetric positive definite tensor. Here the components k^*_{0ij} are derived from

$$v_i = -\frac{k^*_{0ij}}{\eta}G_j, \qquad (23)$$

where v_i are the components of the local velocity field. Similarly to the tortuosity tensor $\alpha_{\infty ij}$, k_{0ij} takes the same values along the x and y axes and can be different along z.

4.2.2. Numerical results and discussions

The permeability of each generated REV described in Section 2 having been calculated, the next objective is to obtain a description for all types of random fibrous media using their single geometrical characteristics r_f, ϕ and Ω_{zz}. As for the electric conduction problem (tortuosity α_∞ and viscous length Λ), a study of the possible effects of anisotropy on the results is conducted. We start however by presenting a classical model, which is used in the following for the analysis of our data.

Several classical models aim at representing the dependence of permeability on the geometrical fiber web characteristics. The most classical model is the Kozeny-Carman equation (see Equation (6) of [28])

$$\frac{k_0}{r_f^2} = \zeta\frac{\phi^3}{(1-\phi)^2}, \qquad (24)$$

where ζ is the Kozeny "constant" which depends on the particle shape and size forming the solid skeleton. As noted in this model, the normalized permeability k_0/r_f^2 is proportional to $\phi^3/(1-\phi)^2$. Consequently, the normalized permeabilities computed on the REVs are plotted in Figure 7 in function of $\phi^3/(1-\phi)^2$.

The numerical results show that the behavior of the permeability tensor k_{0ij} can be different along the (x, y) and z axes. Figure 7 shows that the through-plane normalized permeability k_{0z}/r_f^2 is more sensitive to fiber orientation than the in-plane normalized permeability k_{0xy}/r_f^2.
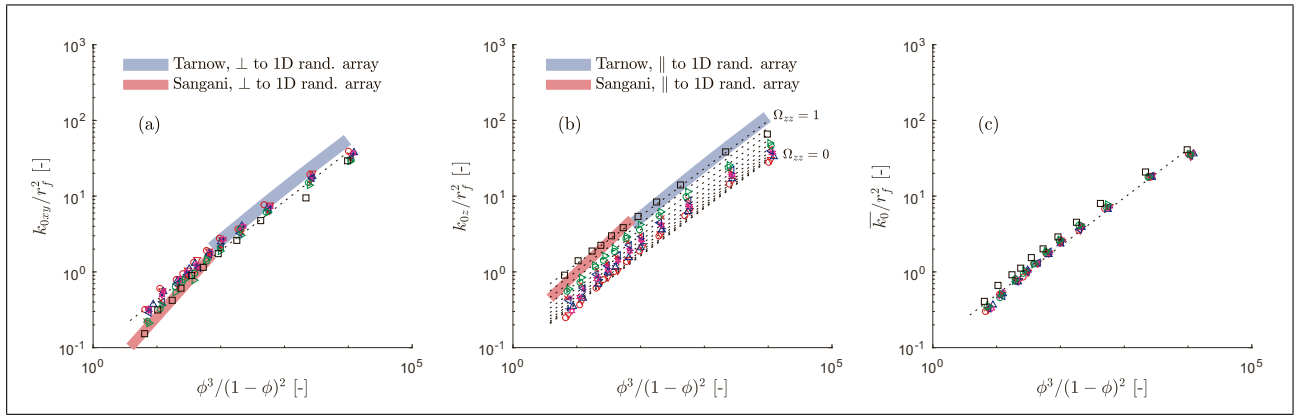
Figure 7. (Colour online) Normalized static viscous permeabilities as a function of $\phi^3/(1-\phi)^2$; (a) k_{0xy}/r_f^2, (b) k_{0z}/r_f^2, (c) $\overline{k}_0/r_f^2$. Same convention of colors and symbols as in Figure 4. The symbols refer to numerically computed values. Dotted lines are estimates obtained by the micro-macro relationships, Equations (25) and (26). Thick blue lines refer to Tarnow's work (Equations (37) and (59) of [3]). Thick pink lines refer to Sangani and Yao's work (Tables II and III of [29]).

Table III. Coefficients of the linear fits to correlate the static viscous permeability tensor k_{0ij} to the porosity function $\phi^3/(1-\phi)^2$.

	k_{0xy}	$\overline{k}_0$
A	0.652	0.640
B	-1.022	-0.941

In view of Figure 7a, in-plane normalized permeability k_{0xy}/r_f^2 varies linearly in function of $\phi^3/(1-\phi)^2$ - this is consistent with Kozeny- Carman equation. Figure 7b suggests that ratio k_{0z}/r_f^2 also depends on the fiber orientation Ω_{zz}. Indeed, the ratio k_{0z}/r_f^2 increases significantly for larger fiber alignment in the direction of the wave propagation $\overrightarrow{e}_3$. Numerical fits can be obtained for k_{0xy}/r_f^2 and $\overline{k}_0/r_f^2$ in the form of

$$\log_{10}\left(\frac{k_0}{r_f^2}\right) = A\log_{10}\left(\frac{\phi^3}{(1-\phi)^2}\right) + B \qquad (25)$$

(valid for $0.75 \leqslant \phi \leqslant 1$).

The effect of fiber orientation appears to be negligeable on the in-plane normalized permeability k_{0xy}/r_f^2 when compared to the through-plane normalized permeability k_{0z}/r_f^2. Some global numerical fits wit Equation (25) can be found for k_{0xy} and $\overline{k}_0$ as linear forms, see Table III for the corresponding coefficients A and B.

A simple expression for estimating the normalized permeability k_{0z}/r_f^2 in function of $\phi^3/(1-\phi)^2$ and fiber orientation Ω_{zz} can take the form of

$$\log_{10}\left(\frac{k_0}{r_f^2}\right) = A\log_{10}\left(\frac{\phi^3}{(1-\phi)^2}\right)$$
$$+ B\Omega_{zz}^2 + C\Omega_{zz} + D \qquad (26)$$

(valid for $0.75 \leqslant \phi \leqslant 1$),

with $A = 0.6295$, $B = 0.4628$, $C = 0.0621$, $D = -1.0482$.

Estimates of k_0/r_f^2 obtained with Equations (25) and (26) are plotted in Figure 7 (dotted lines). As for the tortuosity and the viscous characteristic length, comparison with Equation (12) of Tomadakis and Robertson did not lead to good correlation on all the studied porosity range. Their permeability estimate may be regarded as valid provided that the throat region of the pore space varies relatively slow as one moves away from the throat. However, good comparisons were obtained with results obtained by Tarnow [3] and Sangani and Yao [29] for the 1-d case of a random fiber array; this corresponds to the case of $\Omega_{zz} = 1$ (black squares). This tends to validate our numerical results and micro-macro relationships given by Equations (25) and (26).

In summary, the permeability of a random fibrous medium can be related to the fiber radius r_f, the porosity ϕ, and the angular orientation Ω_{zz}. It can therefore be predicted directly from the knowledge of the microstructural features.

4.3. Static thermal permeability

The thermal terminology is used here but the following developments are also valid for diffusion of Brownian particles whose size is small with respect to a typical size of the medium. Isothermal heat diffusion and Brownian motion in porous media are governed by a Poisson equation,

$$\nabla^2\tau = -1, \qquad (27)$$

where τ is the local field. When the frame has a sufficiently large thermal capacity, the excess temperature τ can be considered to vanish at the fiber walls, and the boundary condition is

$$\tau = 0 \quad \text{on} \quad \partial\Omega. \qquad (28)$$

The excess temperature field τ is spatially periodic. The mean value of the excess temperature field in the fluid
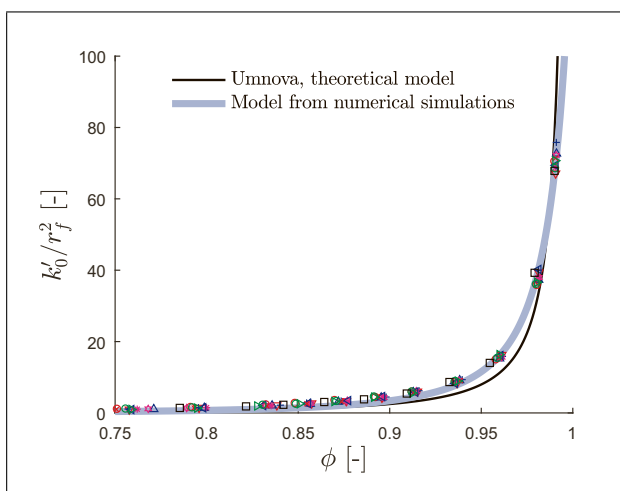
Figure 8. (Colour online) Normalized static thermal permeability k_0'/r_f^2 as a function of porosity ϕ. Same convention of colors and symbols as in Figure 4. The symbols refer to numerically computed values. Thick blue line is the estimate obtained by the micro-macro relationship, Equation (31). Thin black line refers to Umnova *et al.*'s work (Equation (58) of reference [31]).

space between fibers is directly related to the definition of the (scalar) static thermal permeability,

$$k_0' = \langle \tau \rangle. \tag{29}$$

Alternatively, the diffusion controlled trapping constant of the porous frame is given by $\Gamma = 1/k_0'$.

Based on the numerically calculated values of k_0' on the REVs, the normalized thermal permeability k_0'/r_f^2 is shown in Figure 8 as a function of the porosity for the various fiber orientations. Beacause the diffusion of heat does not provide any preferred direction, the static thermal permeability k_0' normalized by the square of the fiber radius r_f^2 can generally be written as a function independant of fiber orientation. In their work, Olny and Panneton [30] provide the following relation between the low-frequency Champoux-Allard description of the thermal characteristic length Λ_{lf}' and the static thermal permeability (Section II.B of [30]),

$$k_0' = \phi \frac{\Lambda_{lf}'^2}{8}. \tag{30}$$

Substituting Λ_{lf}' by Equation (12), one can derive a basic expression for the normalized thermal permeability in function of the open porosity. It is given by

$$\frac{k_0'}{r_f^2} = m_1 \frac{\phi^3}{(1 - \phi + m_2)^2} \tag{31}$$

(valid for $0.75 \leqslant \phi \leqslant 1$).

Values of $m_1 = 0.0691$ and $m_2 = 0.0216$ are obtained by curve-fitting in a least square sense on the simulation results.

Estimates of k_0'/r_f^2 obtained with Equations (31) are plotted in Figure 8 (thick line). For the static thermal permeability, few results are available in the litterature for the types of random fiber structures under study. However, Umnova *et al.* [31] developed a theoretical expression for a 1-d square array of fibers. We present in Figure 8 a comparison between this analytical result and our numerical finite element solution. We see that both estimates agree well.

In summary, the static thermal permeability of a random fibrous medium can be related to the fiber radius r_f, the porosity ϕ, and the angular orientation Ω_{zz}. It can therefore be predicted directly from the knowledge of the microstructural features.

5. Application

In this section, the micro-macro relationships developed earlier are used to investigate the influence of the randomness of the fiber orientation on the acoustical properties. Here, three different nonwoven transversely isotropic fiber assemblies are studied. The first assembly has an open porosity of 0.90 and is composed of fibers having an average diameter of 25 μm (this corresponds to a layer of natural milkweed hollow fibers compacted up to approximately 33.5 kg/m^3). Note that the open porosity is the inter fiber porosity since the hollow part of the fibers it is too small to significantly influence the acoustic behaviour. The fibers are then considered to be solid. Similarly, in the second assembly, the average diameter is 25 μm; however, this time the open porosity is 0.99 (this correspond to a layer of natural milkweed hollow fibers compacted up to approximately 3.35 kg/m^3). The porosity of the third assembly is also 0.99; however, the average fiber diameter is reduced to 10 μm (this corresponds to a light glass fiber of 25 kg/m^3).

Based on the microstructural features r_f and ϕ of the assemblies, the previous micro-macro relationships are used to evaluate the geometrical and transport properties at different angular orientations Ω_{zz} along the z-axis. These relationships are given by Equation (12) for Λ', Equation (17) for α_∞, Equation (19) for Λ, Equation (26) for k_0, and Equation (31) for k_0'. Knowing the fiber radius r_f (in connection with the type of fiber), the fiber orientation Ω_{zz} (in connection with the type of nonwoven manufacturing process), and the open porosity ϕ (in connection with the rate of compaction), these relations completely define the input macroscopic parameters to use in an equivalent fluid model. Here, the six-parameter Johnson-Lafarge equivalent fluid model is used. In this model, the equivalent dynamic density and bulk modulus are respectively given by

$$\rho_{eq} = \frac{\rho_0}{\phi} \left(\alpha_\infty + \frac{\nu\phi}{j\omega k_0} \sqrt{1 + \left(\frac{2\alpha_\infty k_0}{\phi\Lambda} \right)^2 \frac{j\omega}{\nu}} \right) \tag{32}$$

and

$$K_{eq} = \frac{\frac{\gamma P_0}{\phi}}{\gamma - (\gamma - 1) \left(1 + \frac{\phi\nu'}{j\omega k_0'} \sqrt{1 + \left(\frac{2k_0'}{\phi\Lambda'} \right)^2 \frac{j\omega}{\nu}} \right)^{-1}}, \tag{33}$$
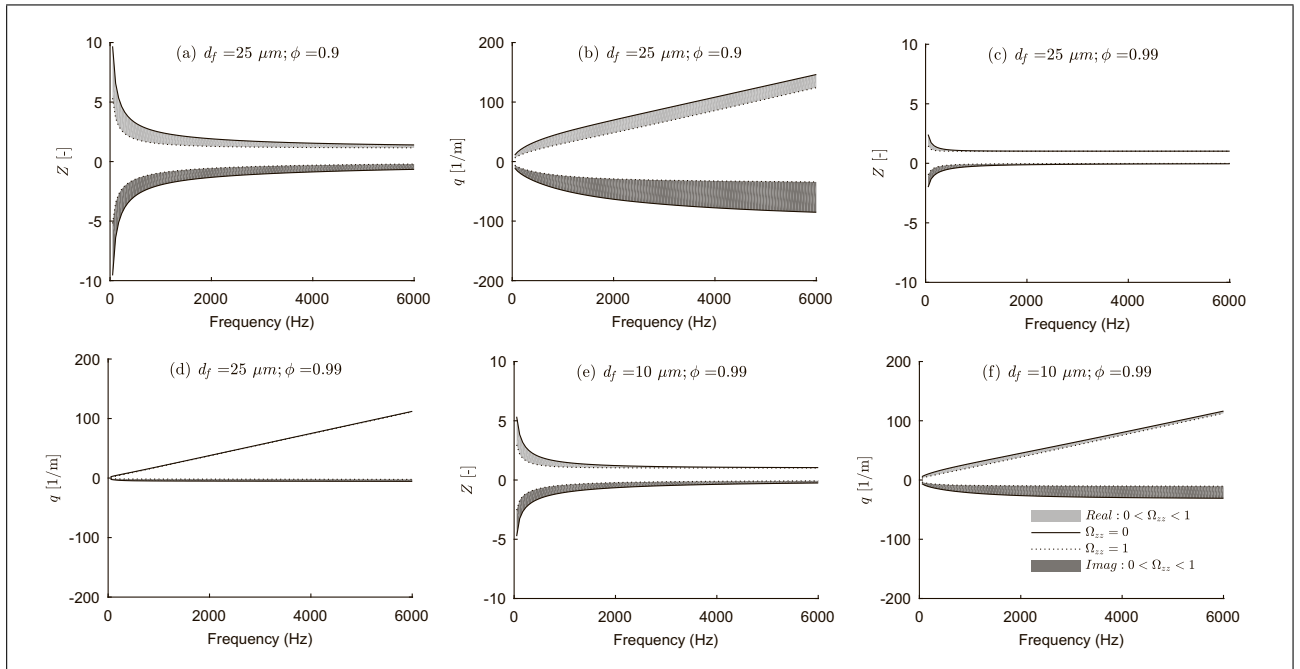
Figure 9. Effects of random fiber orientation on the normalized characteristic impedance (left) and complex wave number (right) for three non-woven fibrous materials with different microstructural features. (a,b) 0.90 porosity with 25 μm fiber diameter. (c,d) 0.99 porosity with 25 μm fiber diameter. (e,f) 0.99 porosity with 10 μm fiber diameter. The grayed area corresponds to the variation of the property between $0 < \Omega_{zz} < 1$, while the solid and dashed lines correspond to $\Omega_{zz} = 0$ and $\Omega_{zz} = 1$, respectively.

where $\nu^{'}$ is the thermal diffusity of the fluid, P_0 is the static pressure, and ω is the angular frequency. From the previous dynamic properties, the normalized characteristic impedance and the complex wavenumber are respectively defined as

$$Z = \frac{1}{\rho_0 c_0} \sqrt{\rho_{eq} K_{eq}} \tag{34}$$

and

$$q = \omega \sqrt{\frac{\rho_{eq}}{K_{eq}}}, \tag{35}$$

where c_0 is the speed of sound in the fluid. Finally, from these two acoustic properties, the normal incidence sound absorption coefficient and transmission loss of a fibrous slab of thickness h are respectively given by

$$\alpha = 1 - \left| \frac{\cos(qh) - \frac{j}{Z}\sin(qh)}{\cos(qh) + \frac{j}{Z}\sin(qh)} \right|^2 \tag{36}$$

and

$$TL = 20 \log_{10} \left| \cos(qh) + \frac{j}{2}\left(Z + \frac{1}{Z}\right)\sin(qh) \right|. \tag{37}$$

Figure 9 presents the normalized characteristic impedance Z and complex wavenumber q for the three materials at different angular orientations Ω_{zz}. One can note that Z and q seem sensitive to the angular orientation for lower porosities, or for smaller fiber diameters. However, for a diameter of 25 μm at a high porosity of 0.99, both Z and

q seem not sensitive to the angular orientation, see Figures 9c and 9d. Only based on these complex acoustic properties, this conclusion may be misleading since for the second case (where Z and q seem not sensitive to orientation), the angular orientation strongly affects the sound absorption coefficient of a 100-mm thick (4 inches) layer as shown in Figure 10c. In fact, comparing Figure 9 with Figure 10, one can conclude that small variations on Z and q, with respect to Ω_{zz}, do not systematically imply small variations on global acoustic indicators such as α and TL.

6. Conclusions

Randomly overlapping fiber structures have been generated from the knowledge of three parameters describing their microstructure: the characteristic fiber radius r_f, the open porosity ϕ, and the fiber orientation coefficient Ω_{zz}. Their macroscopic geometrical and transport properties were numerically calculated on Representative Elementary Volumes (REVs) of the fiber structures. Their dependence on the microstructural parameters were expressed in terms of micro-macro relationships. These relationships are given by Equation (12) for the thermal characteristic length $\Lambda^{'}$, Equation (17) for the tortuosity tensor $\alpha_{\infty ij}$, Equation (19) for the viscous characteristic length tensor Λ_{ij}, Equations (25) and 26 for the static viscous permeability tensor k_{0ij}, and Equation (31) for the static thermal permeability $k_0^{'}$.

The numerical results and the proposed micro-macro relationships were validated by comparison with existing results found in the literature. Contrary to existing results, the new results cover the whole range of fiber orientations.
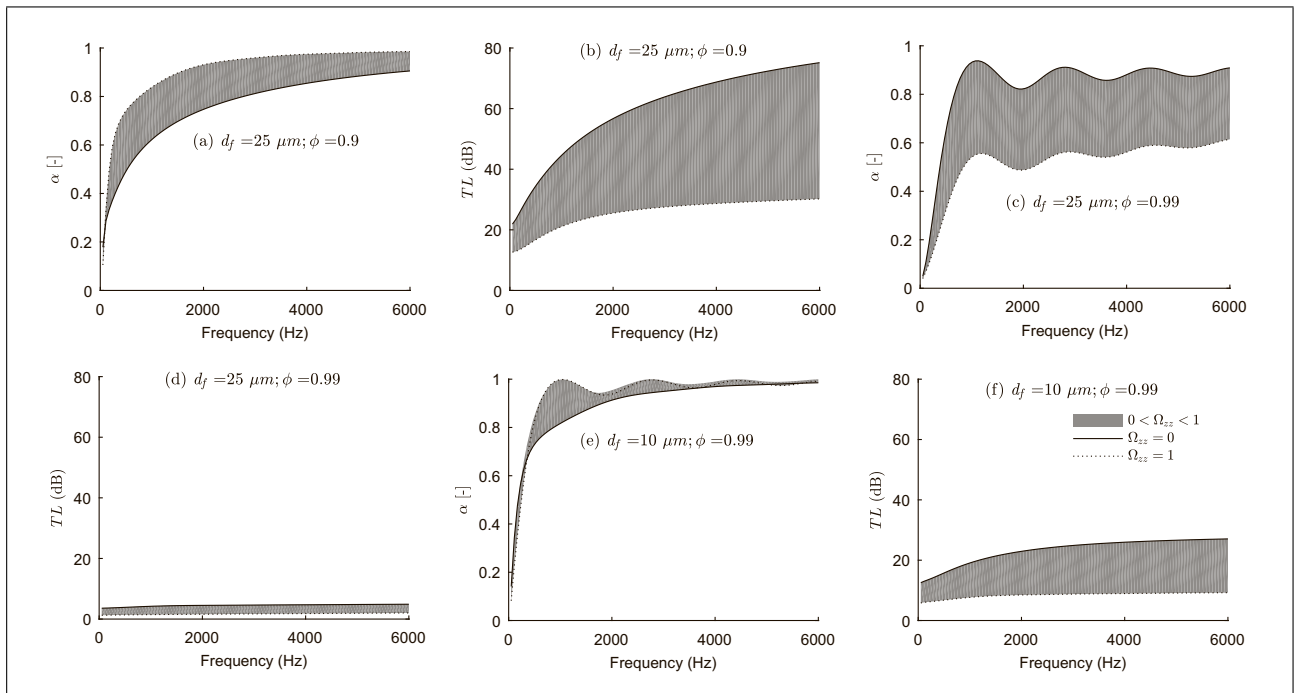
Figure 10. Effects of random fiber orientation on the sound absorption coefficient (left) and sound transmission loss (right) for three non-woven fibrous materials with different microstructural features. (a,b) 0.90 porosity with 25 μm fiber diameter. (c,d) 0.99 porosity with 25 μm fiber diameter. (e,f) 0.99 porosity with 10 μm fiber diameter. The grayed area corresponds to the variation of the property between $0 < \Omega_{zz} < 1$, while the solid and dashed lines correspond to the $\Omega_{zz} = 0$ and $\Omega_{zz} = 1$, respectively.

However, the results are limited to open porosities greater or equal to 0.75. Moreover, some questions remain open concerning the overlapping of the fibers. In fact, in a real fibrous material, the fibers do not really overlap. Nevertheless, due to the possible crushing of the fibers one on the other, it was argued that the overlapping may present more realistic predictions than the non-overlapping case. This argument is also supported by the good comparisons between overlapping model predictions and some experimental data in the review by Tomadakis and Robertson [13].

Finally, the micro-macro relationships were used to study the influence of the fiber orientation Ω_{zz} on the acoustic properties of three specific nonwoven fibrous materials of different porosities and fiber radii. It was found that small variations on the characteristic impedance Z and wave number q, with respect to Ω_{zz}, do not systematically imply small variations on global acoustic indicators such as the sound absorption coefficient α and the sound transmission loss TL - the reverse being also true. Consequently, in order to avoid misinterpretation of the complex influence of the microstructural features on the acoustic behavior, the desired acoustic characteristics, or the microstructural parameters, need to be clearly defined first. In this case, the micro-macro relationships may be very useful to investigate this complex influence between the microstructure and the macroscopic behaviors.

Acknowledgements

References

[1] M. E. Delany, E. N. Bazley: Acoustical properties of fibrous absorbent materials. Appl. Acoust. **3** (1970) 105-116.

[2] Y. Miki: Acoustical properties of porous materials. Modifications of Delany-Bazley models. J. Acoust. Soc. Japan **11** (1990) 19-24.

[3] V. Tarnow: Airflow resistivity of models of fibrous acoustic materials. J. Acoust. Soc. Am. **100** (1996) 3706-3713.

[4] V. Tarnow: Measured anisotropic air flow resistivity and sound attenuation of glass wool. J. Acoust. Soc. Am. **111** (2002) 2735-2739.

[5] M.-Y. Zhou, P. Sheng. First-principles calculations of dynamic permeability in porous media. Phys. Rev. B. **39** (1989) 12027-12039.

[6] R. J. Brown: Connection between formation factor for electrical resistivity and fluid-solid coupling factor in Biot's equations for acoustic waves in fluid-filled porous media. Geophys. **45** (1980) 1269-1275.

[7] Lord Rayleigh: On the influence of obstacles arranged in rectangular order upon the properties of a medium. Philos. Mag. **34** (1892) 481-502.

[8] D. L. Johnson, J. Koplik, L. M. Schwartz: New pore-size parameter characterizing transport in porous media Phys. Rev. Lett. **57** (1986) 2564-2567.

[9] D. L. Johnson, J. Koplik, R. Dashen: Theory of dynamic permeability and tortuosity in fluid-saturated porous media. J. Fluids. Mech. **176** (1987) 379-402.

[10] D. Lafarge, P. Lemarinier, J. F. Allard, V. Tarnow: Dynamic compressibility of air in porous structures at audible frequencies. J. Acoust. Soc. Am. **102** (1997) 1995-2006.

[11] J.-F. Allard, Y. Champoux: New empirical equations for sound propagation in rigid frame fibrous materials. J. Acoust. Soc. Am. **91** (1992) 3346-3353.

[12] S. G. Advani, C. L. Tucker: The Use of Tensors to Describe and Predict Fiber Orientation in Short Fiber Composites. J. Rheol. **31** (1987) 751-784.

[13] M. M. Tomadakis, T. J. Robertson: Viscous permeability of random fiber structures: Comparison of electrical and diffusional estimates with experimental and analytical results. J. Comp. Mat. **39** (2005) 163-188.

[14] K. Schladitz, S. Peters, D. Reinel-Bitzer, A. Wiegmann, J. Ohser: Design of acoustic trim based on geometric modeling and flow simulation for non-woven. Comp. Mat. Sci. **38** (2006) 56-66.

[15] C. Jensen, R. Raspet: Design of acoustic trim based on geometric modeling and flow simulation for non-woven. J. Acoust. Soc. Am. **127** (2010) 3470-3484.

[16] H.-S. Roh, R. Raspet, H. E. Bass: Parallel capillary-tube-based extension of thermoacoustic theory for random porous media. J. Acoust. Soc. Am. **121** (2007) 1413-1422.

[17] D. K. Wilson: Relaxation-matched modeling of propagation through porous media, including fractal pore structure. J. Acoust. Soc. Am. **94** (1993) 1136-1145.

[18] H. Brenner: Rheology of a dilute suspension of axisymmetric Brownian particles. Int. J. Multiphase Flow. **1** (1974) 195-341.

[19] R. B. Bird, R. C. Amstrong, O. Hassager, C. F. Curtiss: Dynamics of polymeric liquids. Vol. 2: Kinetic theory. 2nd Ed. Wiley, New York, 1987, pp. 464.

[20] E. J. Hinch, L. G. Leal: Constitutive equations in suspension mechanics. Part 1. General formulation. J. Fluid. Mech. **76** (1975) 481-495.

[21] E. J. Hinch, L. G. Leal: Constitutive equations in suspension mechanics. Part 2. Approximate forms for a suspension of rigid particles affected by Brownian rotations. J. Fluid. Mech. **76** (1977) 187-208.

[22] H. T. Luu, C. Perrot, V. Monchiet, R. Panneton: Three-dimensional reconstruction of a random fibrous medium: geometry, transports, and acoustical properties. J. Acoust. Soc. Am. **141** (2017) 4768-4780.

[23] A. I. Abd El-Rahman, C. L. Tucker III: Mechanics of random discontinuous long-fiber thermoplastics. Part I: Generation and characterization of initial geometry. J. Appl. Mech. **80** (2013) 051007-10.

[24] L. L. Beranek: Acoustic impedance of porous materials. J. Acoust. Soc. Am. **13** (1942) 248-260.

[25] R. Panneton, E. Gros: A missing mass method to measure the open porosity of porous solids. Acta Acust. united Ac. **91** (2005) 342-348.

[26] Y. Salissou, R. Panneton: Pressure/mass method to measure open porosity of porous solids. J. Appl. Phys. **101** (2007) 124913-7.

[27] H. T. Luu, R. Panneton, C. Perrot: Effective fiber diameter for modeling the acoustic properties of polydisperse fiber networks. J. Acoust. Soc. Am. **141** (2017) EL96-EL101.

[28] M. T. Pelegrinis, K. V. Horoshenkov, A. Burnett: An application of Kozeny-Carman fow resistivity model to predict the acoustical properties of polyester fibre. Appl. Acoust. **101** (2016) 1-4.

[29] A. S. Sangani, C. Yao: Transport processes in random arrays of cylinders. II. Viscous flow. Phys. Fluids **31**(9) (1988) 2435-2444.

[30] X. Olny, R. Panneton: Acoustical determination of the parameters governing thermal dissipation in porous media. J. Acoust. Soc. Am. **123** (2008) 814-824.

[31] O. Umnova, D. Tsiklauri, R. Venegas: Effect of boundary slip on the acoustical properties of microfibrous materials. J. Acoust. Soc. Am. **126** (2009) 1850-1861.